This article has been accepted for publication in a future issue of this journal, but has not been fully edited. Content may change prior to final publication. Citation information: DOI 10.1109/JLT.2018.2879483, Journal of Lightwave Technology

A Microwave Photonics Equalizer for Overcoming Dispersion-Induced Distortions on Wideband Signals in Radio-over-Fiber Links

Guanyu Han, Shangyuan Li, Haojie Wang, Xiaoxiao Xue, and Xiaoping Zheng

***Abstract*—Chromatic dispersion (CD) has been considered as a significant issue that needs to be addressed over the past decades. Nowadays, as the bandwidth of radio frequency (RF) signals has expanded to multi-gigahertz, CD becomes increasingly troublesome for some wideband signals such as linear frequency modulated waveform (LFMW), which requires a flat amplitude response and a linear phase response. In this paper, we firstly investigate the CD-induced amplitude distortion and phase distortion that a wideband signal will suffer in traditional double-sideband (DSB) modulated and single-sideband (SSB) modulated RoF links with an emphasis on the LFMW. The detrimental impacts of the CD-induced distortions are subsequently discussed based on the pulse compression performance. Then, a 2-tap microwave photonics equalizer (MPE) model is proposed and its operating principle for overcoming the CD-induced distortions is demonstrated. Based on the model, we design the MPE, which is mainly composed of an integrated dual-polarization dual-parallel Mach-Zehnder modulator (DP-DPMZM) and a differential group delay (DGD) module. In the proof-of-concept experiment, the RoF link utilizing the proposed MPE is built, and a 1-10 GHz LFMW is transmitted over the 66.3 km single-mode fiber (SMF). Thanks to the MPE, both CD-induced amplitude distortion and phase distortion are successfully compensated. Pulse compression results show that the pulse fission which will happen in the traditional DSB-based link is avoided. The compressed pulse is less broadened and its peak sidelobe ratio has a 3.23 dB improvement, compared with the signal transmitted in the SSB-based link.**

***Index Terms*—Chromatic dispersion, radio over fiber, equalizer**

I. Introduction

RADIO-OVER-FIBER (RoF) has become an attractive technique for signal transmission over the past decades because of its low transmission loss, immunity to electromagnetic interference, and broad bandwidth [1]. Despite these merits above, numerous issues still exist. One major problem which needs to be addressed is the distortions introduced by chromatic dispersion (CD). For an RoF link, the fiber-induced CD causes different spectral components to travel at different velocities, which results in relative phase differences between the carrier and sidebands [2]. Consequently, for the traditional double sideband (DSB) modulated link, the cancellation between the two beat signals happens at certain frequencies and it distorts the amplitude response of the link. In this case, the transmission distance and operation bandwidth are severely limited [3].

Many methods aiming to overcome the CD effect have been proposed. Several devices such as dispersion compensation fiber [4], chirped fiber Bragg grating [5] and optical filter [6] are designed for CD compensation. However, these techniques not only reduce the system flexibility but also introduce some unexpected problems such as nonlinearity.

Single sideband (SSB) modulation is considered as an effective approach for overcoming the CD-induced amplitude distortion [7-9]. Whereas, the frequency-dependent group delay derived from CD cannot be removed and will lead to phase distortion, which is a significant handicap for some phase sensitive applications [10].

In our previous work [11], the fading points at specific frequencies are successfully shifted by using the carrier phase-shifted double sideband (CPS-DSB) modulation based on a dual-parallel Mach-Zehnder modulator (DPMZM). Other similar schemes using various modulators and modulation formats are proposed [12-14]. Nevertheless, these methods can only compensate the amplitude distortion at a limited frequency band.

Several transmitters and receivers based on modulation-diversity have been proposed to realize the broadband CD compensation [15-17]. The basic idea of these approaches is to create two complementary responses. After combining them, the distorted amplitude response can be compensated and a flat link response can be achieved. However, in principle, the combined response is a periodic function that still produces amplitude distortion and nulls [18].

Furthermore, since the signal bandwidth has currently increased up to multi-gigahertz, the aforementioned advantages make the RoF technique one of the excellent candidates for wideband signals distribution from the central station to multiple access points [19-21]. However, when such wideband

This work was supported by the National Nature Science Foundation of China under Grants 61690191/2, 61420106003, 61427813, and 61621064, in part by the Chuanxin Funding, and in part by the Beijing Natural Science Foundation under Grant 4172029.

The authors are with the Beijing National Research Center for Information Science and Technology, Department of Electronic Engineering, Tsinghua University, Beijing 100084, China (e-mail: syli@mail.tsinghua.edu.cn;).

Copyright (c) 2015 IEEE. Personal use of this material is permitted. However, permission to use this material for any other purposes must be obtained from the IEEE by sending a request to pubs-permissions@ieee.org.

0733-8724 (c) 2018 IEEE. Personal use is permitted, but republication/redistribution requires IEEE permission. See http://www.ieee.org/publications_standards/publications/rights/index.html for more information.

This article has been accepted for publication in a future issue of this journal, but has not been fully edited. Content may change prior to final publication. Citation information: DOI 10.1109/JLT.2018.2879483, Journal of Lightwave Technology

signals are transmitted over the RoF link, CD will be a significant factor that affects the signal performance. For example, the wideband linear frequency modulated waveform (LFMW), which is a typical wideband signal and is widely used in high-resolution radar systems [24-26], is sensitive to both amplitude and phase distortions. Unfortunately, to our best knowledge, no previous research has focused on this issue.

In section II, we theoretically explore the impacts of CD-induced distortions on the wideband signal in DSB-based and SSB-based RoF links through the analysis of the LFMW. In the traditional DSB-based RoF link, the signal suffers from amplitude distortion which finally results in the pulse fission for the wideband LFMW in pulse compression. Although this amplitude distortion can be removed by SSB modulation, the frequency-dependent group delay derived from CD distorts the phase of the signal. For the LFMW, the CD-induced phase distortion changes the chirp rate and thus the main lobe width (MLW) and the peak sidelobe ratio (PSR) in pulse compression are simultaneously worsened. To overcome the CD-induced distortions, in section III, the model of a 2-tap microwave photonics equalizer (MPE) is proposed. The CPS-DSB modulation is performed in each tap and the weighting coefficients at specific frequencies are determined by the phase shift of optical carrier [11]. Properly adjusting the coefficients and the relative time delay between the two taps, the wideband signal can be transmitted over the RoF link with little CD-induced distortion. In the proof-of-concept experiment (section IV), the MPE is designed, which mainly consists of an integrated dual-polarization dual-parallel Mach-Zehnder modulator (DP-DPMZM) and a differential group delay (DGD) module. The weighting coefficients and the time delay are tunable by adjusting the biases of the DP-DPMZM and the DGD module. Employing the MPE, a 1-10 GHz LFMW is transmitted over the 66.3 km single-mode fiber (SMF). Both amplitude and phase distortions caused by CD are well compensated with the help of the MPE. In section V, we firstly discuss the amplitude ripple, which is a function of three parameters of the MPE. Then a comparison of phase distortion in DSB-based, SSB-based and MPE-based links is made. The CD-induced phase distortion is much more severe in SSB-based link, which makes it not appropriate to transmit phase-sensitive signals. Finally, we compare the performance degradation of the LFMW in three links when the signal is transmitted over different lengths of fiber. The MLW and the PSR in pulse compression are evaluated as functions of the fiber length. By comparison, the MPE reveals its better anti-dispersion performance, denoting that the wideband signal will experience less distortion when the MPE is utilized in the RoF link.

II. CD Effect on Wideband Signal

In this section, we will analyze the CD-induced distortions on a 1-15 GHz LFMW in traditional DSB-based and SSB-based RoF links. In both cases, pulse compression of the output LFMW is performed through the correlation with the input undistorted LFMW. To evaluate the signal performance, the pulse compression results are compared with the ideal one whose MLW is the reciprocal of the bandwidth and PSR is 13.3-dB [24].

A. CD-induced amplitude distortion in the DSB-based link

In general, an LFMW with bandwidth B and duration T can be expressed as [24]

$$S(t) = \cos(\omega_s t + \pi k t^2) \tag{1}$$

$$S(\omega) \propto \exp[-j\frac{(\omega-\omega_s)^2}{k}] \tag{2}$$

where ω_s and $k = B/T$ represent the starting angular frequency and the chirp rate with respective.

For the conventional DSB-modulated link, if the MZM is biased at quadrature, the optical carrier that is centered at ω_c and modulated by $S(t)$ can be written as

$$E_1(t) = E_0 \exp(j\omega_c t)\cos[m\cos(\omega_s t + \pi k t^2) + \frac{\pi}{4}] \tag{3}$$

where E_0 denotes the amplitude of the optical carrier and $m=\pi V_s / 2V_\pi$ is the modulation depth with V_π being the half-wave voltage.

Applying Jacobi-Anger expansion to (3), for the small signal ($m \ll 1$), we neglect the high-order sidebands and rewrite the optical field as

$$E_1(t) \propto E_0 \exp(j\omega_c t)[J_0(m) - J_1(m)\cos(\omega_s t + \pi k t^2)] \tag{4}$$

where $J_n(\bullet)$ is the first kind Bessel function of order n.

Taking the fiber-induced CD into consideration and neglecting the high-order dispersion, the transfer function of the SMF with length L is [2]

$$H(\omega) \propto \exp[j\frac{1}{2}\beta_2 L(\omega-\omega_c)^2] \tag{5}$$

where β_2 is the dispersion coefficient of the SMF.

At the output end, the LFMW feeding to the photodetector (PD) is given as

$$E_2(t)=\Im^{-1}[E_1(\omega)H(\omega)] \propto \left\{\begin{array}{l} J_0(m)\exp(j\omega_c t) \\ -J_1(m)\exp\, j[(\omega_c+\omega_s)t + \dfrac{\pi k}{1-\beta_2 Lk/2}t^2 - \dfrac{1}{2}\beta_2 L\omega_s^2] \\ -J_1(m)\exp\, j[(\omega_c-\omega_s)t - \dfrac{\pi k}{1+\beta_2 Lk/2}t^2 - \dfrac{1}{2}\beta_2 L\omega_s^2] \end{array}\right\} E_0 \tag{6}$$

where $\Im^{-1}(\bullet)$ is the inverse Fourier transform operation.

As a result, the output LFMW field is:

$$\begin{aligned} I_{DSB}(\omega) &\propto \cos\frac{1}{2}\beta_2 L[(\omega-\omega_s)^2 - \omega_s^2]\exp[-j\frac{(\omega-\omega_s)^2}{k}] \\ &= \cos\frac{1}{2}\beta_2 L[(\omega-\omega_s)^2 - \omega_s^2] I_{in}(\omega) \end{aligned} \tag{7}$$

where $I_{in}(\omega)$ is the spectrum of the input signal. It can be seen that in a traditional DSB-based RoF link, a cos-like envelope is

Copyright (c) 2015 IEEE. Personal use of this material is permitted. However, permission to use this material for any other purposes must be obtained from the IEEE by sending a request to pubs-permissions@ieee.org.

0733-8724 (c) 2018 IEEE. Personal use is permitted, but republication/redistribution requires IEEE permission. See http://www.ieee.org/publications_standards/publications/rights/index.html for more information.

This article has been accepted for publication in a future issue of this journal, but has not been fully edited. Content may change prior to final publication. Citation information: DOI 10.1109/JLT.2018.2879483, Journal of Lightwave Technology

applied to the input LFMW and it will lead to the amplitude distortion.

Fig. 1 shows the frequency spectra of the 1-15 GHz LFMW transmitted over different distances in simulation. Notch points appear at 13.55- and 9.58-GHz when the LFMW is transmitted over the 20- and 40-km SMF, respectively.

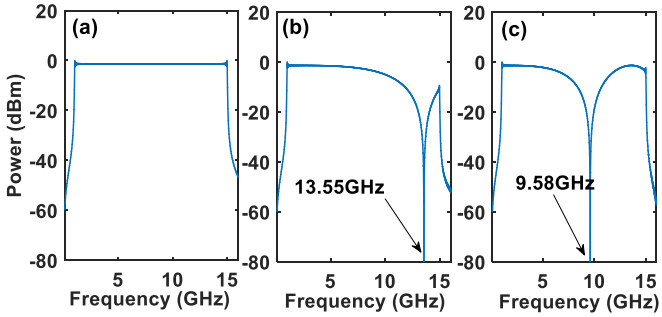

Fig. 1. Frequency spectra of the 1-15 GHz LFMW transmitted over (a) 0 km, (b) 20 km and (c) 40 km SMF in the DSB-based RoF link.

Fig. 2 illustrates the pulse compression results of the wideband LFMW after transmission over different distances. When the signal is transmitted over a relatively short distance, the amplitude of the signal distorts slightly and the distortion can be equivalent to a window, which lowers the side lobes and broadens the MLW simultaneously (Fig. 2(b)) [24]. As the transmission distance increases, the LFMW suffers from more serious amplitude distortion as is shown in Fig. 1(c) and the pulse fission happens as is shown in Fig. 2 (c), which means a false target is introduced.

The physical explanation of the pulse fission is illustrated as follows. Due to the fiber-induced CD, the upper and lower sidebands have different time delays with respect to the optical carrier after transmission. The output LFMW, as a result, is equivalent to the sum of two sub-LFMWs, which have different time delays relative to the original signal. Correspondingly, the compressed pulse can be regarded as the combination of two sub-pulses, whose peaks are separated in time because of their different time delays. When the signal is transmitted in a short distance, the time difference between the separated two sub-pulses is less than a single resolution cell (the MLW of the ideal compressed pulse [24]) so that the compressed pulse maintains the shape but has a broadening main lobe. With the increasing of the fiber length, their time difference gradually increases and eventually exceeds a resolution cell. Consequently, the two sub-pulses can be discriminated and the pulse fission happens as is shown in Fig. 2(c).

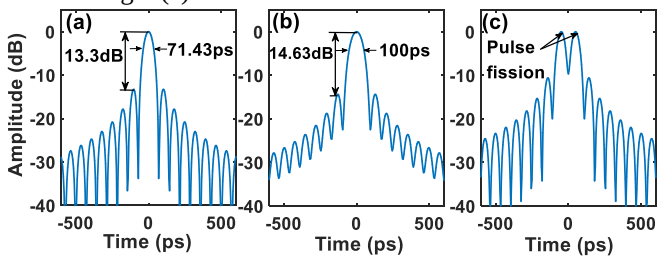

Fig. 2. Pulse compression results of the 1-15 GHz LFMW transmitted over (a) 0-km (b) 20-km and (c) 40-km SMF in the DSB-based RoF link.

B. CD-induced phase distortion in the SSB-based link

For the SSB-based RoF link, albeit the amplitude distortion can be eliminated, the phase distortion introduced by CD cannot be evaded. Supposing the lower sideband is removed, we rewrite the equation (6) as

$$E_2(t) \propto \left\{ \begin{array}{l} J_0(m)\exp(j\omega_c t) - \\ J_1(m)\exp j[(\omega_c+\omega_s)t + \dfrac{\pi k}{1-\beta_2 Lk/2}t^2 - \dfrac{1}{2}\beta_2 L\omega_s^2] \end{array} \right\} E_0 \tag{8}$$

Hence, the output LFMW field is

$$I_{SSB}(\omega) \propto \exp j[-\frac{(\omega-\omega_s)^2}{k/(1-\beta_2 Lk/2)} - \frac{1}{2}\beta_2 L\omega_s^2] \tag{9}$$

It can be seen that the amplitude distortion is removed. Nevertheless, the non-constant group delay caused by CD changes the chirp rate of the output LFMW and it finally leads to the phase distortion.

This phase distortion results in the degradation of signal performance, which can be verified by pulse compression. As is demonstrated in Fig. 3, the phase distortion not only contributes to the broadening of the main lobe but also reduces the PSR. Consequently, the resolution is worsened (main lobe broadening) and the capacity of detecting small targets is deteriorated (the reduction of PSR) at the same time.

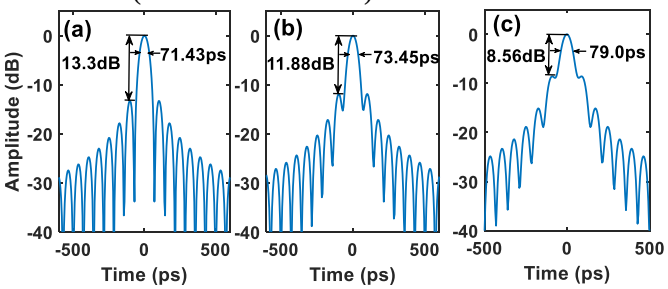

Fig. 3. Pulse compression results of the 1-15 GHz LFMW transmitted over (a) 0 km (b) 40 km and (c) 80 km SMF in the SSB-based RoF link.

III. MPE Model and Principle

To overcome the CD-induced distortions, we propose the MPE model. The schematic model of the MPE is presented in Fig. 4.

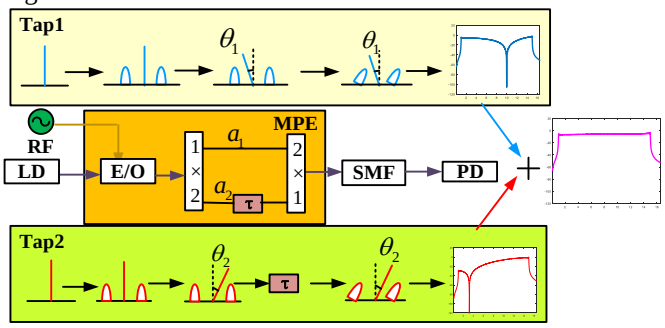

Fig. 4. Schematic model of the proposed 2-tap MPE. RF: radio frequency. LD: laser diode. MPE: microwave photonics equalizer. SMF: standard-mode fiber. PD: photodetector.

Based on the previous analysis, the SSB modulation can lead to the deviation of the chirp rate and will result in the phase distortion. Thus, we adopt the DSB modulation for the MPE to

Copyright (c) 2015 IEEE. Personal use of this material is permitted. However, permission to use this material for any other purposes must be obtained from the IEEE by sending a request to pubs-permissions@ieee.org.

0733-8724 (c) 2018 IEEE. Personal use is permitted, but republication/redistribution requires IEEE permission. See http://www.ieee.org/publications_standards/publications/rights/index.html for more information.

This article has been accepted for publication in a future issue of this journal, but has not been fully edited. Content may change prior to final publication. Citation information: DOI 10.1109/JLT.2018.2879483, Journal of Lightwave Technology

ensure there is no CD-induced phase distortion. Accordingly, the CPS-DSB technique can manipulate the amplitude response by controlling the phase shift of the optical carrier, and thus the weighting coefficients at specific frequencies can be manipulated [11]. Therefore, we apply the CPS-DSB modulation in the taps of the MPE to control the weighting coefficients of each tap.

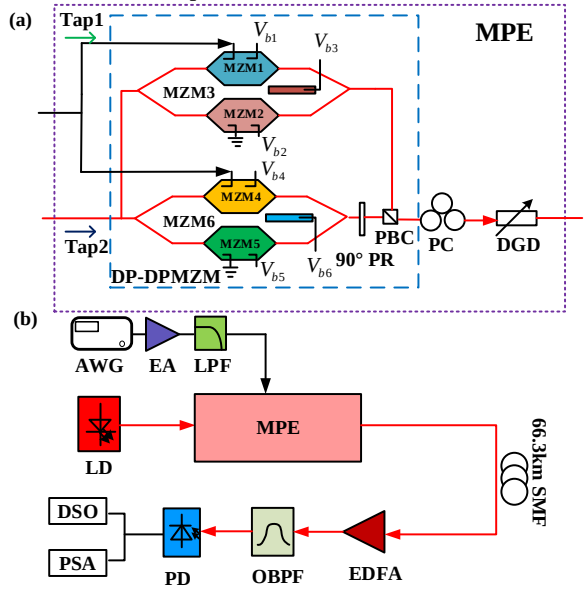

Fig. 7. (a) Detailed structure of the MPE. (b) Experimental setup of the MPE-based RoF link. PR: polarization rotator. PBC: polarization beam combiner. PC: polarization controller. DGD: differential group delay. DP-DPMZM: dual-polarization dual-parallel Mach-Zehnder modulator. AWG: arbitrary waveform generator. EA: electrical amplifier. LPF: low-pass filter. EDFA: erbium-doped fiber amplifier. OBPF: optical band-pass filter. DSO: digital storage oscilloscope. PSA: power spectrum analyzer. MPE: microwave photonics equalizer.

As is shown in Fig. 4, the RF signal is firstly modulated onto the optical carrier. Subsequently, two independent taps are generated in the equalizer. In each tap, the tunable CPS-DSB modulation is performed. For the tap i, the MPE introduces an initial phase shift θ_i to the optical carrier before transmission. After transmission, the fiber-induced CD causes the phase shift $\phi(\omega)=\beta_2 L[(\omega-\omega_s)^2-\omega_s^2]/2$ to both upper sideband and lower sideband with respect to the optical carrier. Therefore, the relative phase difference between the optical carrier and sidebands at the receive end is:

$$\Delta\varphi_i(\omega)=\phi(\omega)-\theta_i \tag{10}$$

In a DSB-based link, this relative phase difference is converted to an amplitude envelope after photodetection, which can be regarded as the weighting coefficients:

$$W_i(\omega)=\cos[\Delta\varphi_i(\omega)]=\cos\{\frac{1}{2}\beta_2 L[(\omega-\omega_s)^2-\omega_s^2]-\theta_i\} \tag{11}$$

Considering the time delay τ_i, the output LFMW field for the tap i is:

$$\begin{aligned} I_i(\omega) &= A_i W_i(\omega)\exp[-j\frac{(\omega-\omega_s)^2}{k}]\exp(-j\omega\tau_i) \\ &= A_i\cos[\phi(\omega)-\theta_i]\exp[-j\frac{(\omega-\omega_s)^2}{k}]\exp(-j\omega\tau_i) \end{aligned} \tag{12}$$

Assuming that $A_1=A_2=A$, $\tau_1=0$ and τ represents the relative time delay between the two taps, the combined output LFMW field is

$$I_{out}(\omega)\propto\left\{\begin{matrix}\cos[\phi(\omega)-\theta_1]\exp(-j\omega\tau)\\+\cos[\phi(\omega)-\theta_2]\end{matrix}\right\}\exp[-j\frac{(\omega-\omega_s)^2}{k}] \tag{13}$$

According to the previous discussion, when DSB modulation is performed, the relative phase difference between the sidebands and the carrier is converted to the amplitude distortion. Therefore, we concern the amplitude of the output signal:

$$\begin{aligned} P_{out}(\omega) &= |I_{out}(\omega)|^2 \\ &= \left\{\begin{matrix}\cos^2[\phi(\omega)-\theta_1]+\cos^2[\phi(\omega)-\theta_2]\\+2\cos[\phi(\omega)-\theta_1]\cos[\phi(\omega)-\theta_2]\cos\omega\tau\end{matrix}\right\}P_{in}(\omega) \end{aligned} \tag{14}$$

Apparently, when fading points at certain frequencies appear in only one tap ($\cos[\phi(\omega)-\theta_1]=0$ and $\cos[\phi(\omega)-\theta_2]\neq 0$ for example), they can be canceled by the other tap after combination. The additional term $\cos\omega\tau$ in (14) plays a role much like an interleaver which smooths out the amplitude fluctuation. Properly adjusting θ_1, θ_2 and τ, fading points can be eliminated and the amplitude ripple can be mitigated within 3-dB. However, the slight time delay between the two taps will introduce a phase error, which may cause the degradation of signal performance. In this scenario, a reasonable compensation strategy is to minimize τ and meanwhile find appropriate θ_1, θ_2 to achieve the optimal solution.

Fig. 5 illustrates the compensation results of the 1-15 GHz LFMW transmitted over 20 km, 40 km and 80 km SMF in simulation using the proposed MPE model. As is shown, severe amplitude distortion is well compensated and the maximum amplitude fluctuation is controlled less than 3-dB.

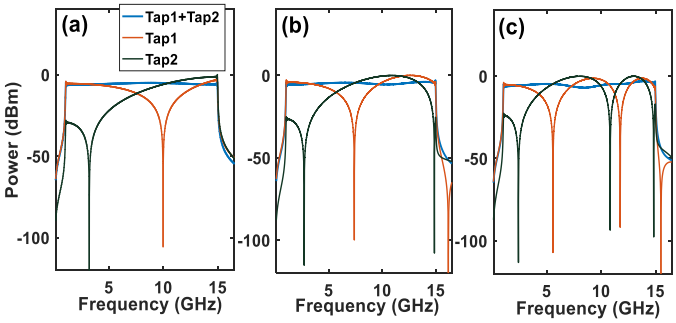

Fig. 5. Frequency spectra of the 1-15 GHz LFMW transmitted over (a) 20 km ($\theta_1=0.71\pi$, $\theta_2=-0.2\pi$ and $\tau=3$ps), (b) 40 km ($\theta_1=0.71\pi$, $\theta_2=-0.2\pi$ and $\tau=4$ps) and (c) 80 km SMF ($\theta_1=0.71\pi$, $\theta_2=-0.2\pi$ and $\tau=4$ps) when the MPE model is applied.

The corresponding pulse compression results are presented in Fig. 6. As is shown, because the amplitude distortion is well compensated, the pulse fission does not happen for the

Copyright (c) 2015 IEEE. Personal use of this material is permitted. However, permission to use this material for any other purposes must be obtained from the IEEE by sending a request to pubs-permissions@ieee.org.

0733-8724 (c) 2018 IEEE. Personal use is permitted, but republication/redistribution requires IEEE permission. See http://www.ieee.org/publications_standards/publications/rights/index.html for more information.

This article has been accepted for publication in a future issue of this journal, but has not been fully edited. Content may change prior to final publication. Citation information: DOI 10.1109/JLT.2018.2879483, Journal of Lightwave Technology

wideband LFMW with the increase of the transmission distance. On the other hand, although the MLW remains unaffected for different transmission distances, there is a degradation in PSR, which results from the slight relative time delay τ between the two taps. This pulse compression results denote that the MLW and PSR will not be deteriorated at the same time when the MPE is applied, which should be considered as a significant advantage over the SSB technique.

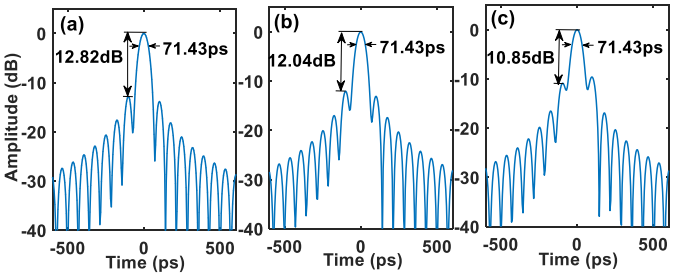

Fig. 6. Pulse compression results of the 1-15 GHz LFMW transmitted over (a) 20-km (b) 40-km and (c) 80-km SMF in the MPE-based RoF link.

IV. Experimental Setup and Results

Based on the proposed model, a 2-tap MPE is designed and an RoF link based on the MPE is built. The detailed structure of the MPE and the experimental setup are shown in Fig. 7.

The MPE mainly consists of an integrated DP-DPMZM (FUJITSU, FTM7977HQA/303), a polarization controller (PC) and a DGD module. The two taps are generated in the integrated DP-DPMZM, which is composed of a 3-dB optical coupler (OC), two identical DPMZMs, a 90-degree polarization rotator (PR), and a polarization beam combiner (PBC).

The CPS-DSB modulation in each tap is performed by the single-drive DPMZM [11], which is consisted of two sub-MZMs and a parent MZM. The sub-MZMs (MZM1, MZM4), which are driven by the input LFMW, are biased at null point and the sub-MZMs (MZM2, MZM5) which have no driven signals are biased at the maximum point. The optical carrier shift θ_1 and θ_2 can be respectively adjusted by tuning the bias voltages V_{b3} and V_{b6}. Since the two DPMZMs are identical, we assume they have the same half-wave voltage $V_{\pi p}$ for the parent MZMs (MZM3, MZM6). Therefore, the θ_1 and θ_2 can be expressed as: $\theta_1 = \pi V_{b3} / V_{\pi p}$ and $\theta_2 = \pi V_{b6} / V_{\pi p}$.

A 1-10 GHz LFMW is generated from an arbitrary waveform generator (AWG) (Tektronix, AWG70002A). An electrical amplifier (EA) with 30 dB gain is used to amplify the input LFMW. To filter out the unexpected spurs and image frequencies, a low-pass filter whose passband is 0-10 GHz is cascaded after the EA. Afterward the LFMW is fed to a 3-dB power splitter as the microwave input of the MPE.

A continuous light wave with the power of 13 dBm is launched from a laser module (OEwaves, OE4032) and then it is input into the DP-DPMZM where two independent CPS-DSB modulated signals are generated and combined. To introduce and adjust the relative time delay between the two taps, a tunable DGD module with tuning capability from -45 to 45 ps and resolution of 0.5 ps, is exploited. Meanwhile, a PC is placed between the DP-DPMZM and the DGD module so that the two orthogonal signals can be aligned to the slow and fast axes of the DGD module.

After being transmitted over the 66.3-km SMF, the optical signal is amplified by an erbium-doped fiber amplifier (EDFA) to compensate the power loss, and an optical band-pass filter (OBPF) is followed to filter the amplified spontaneous emission (ASE) noise. Finally, the frequency spectrum of the output wideband LFMW is measured by a power spectrum analyzer (PSA, Agilent E4446A) and the temporal waveform is sampled by a digital storage oscilloscope (DSO, Agilent DSO81204B).

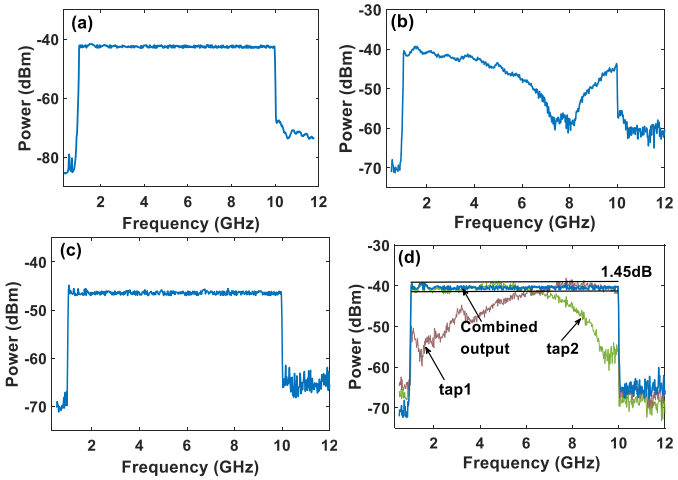

Fig. 8. Measured spectra of the 1-10 GHz LFMW after transmission (a) without SMF, over the 66.3-km SMF in the (b) DSB-based link, (c) SSB-based link and (d) MPE-based link.

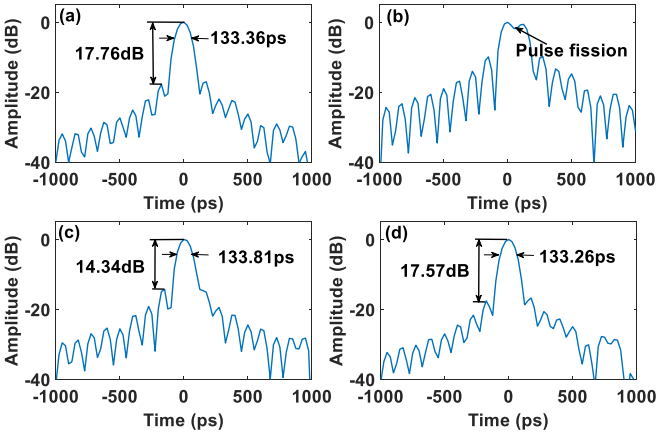

Fig. 9. Pulse compression results of the 1-10 GHz LFMW after transmission (a) without fiber, over 66.3-km SMF in the (b) DSB-based link, (c) SSB-based link and (d) MPE-based link.

Fig. 8 presents the measured the power spectra of the LFMW being transmitted over different fiber lengths. As is manifested in Fig. 8(b), the LFMW experiences serious amplitude distortion in the conventional DSB-based RoF link and the fading point appears around 7.6 GHz. As expected, the amplitude distortion is successfully eliminated by using the SSB modulation (Fig. 8(c)). In the MPE-based link, by tuning the DGD module to adjust the relative time delay and the biases of the DP-DPMZM to manipulate the weighting coefficients,

Copyright (c) 2015 IEEE. Personal use of this material is permitted. However, permission to use this material for any other purposes must be obtained from the IEEE by sending a request to pubs-permissions@ieee.org.

0733-8724 (c) 2018 IEEE. Personal use is permitted, but republication/redistribution requires IEEE permission. See http://www.ieee.org/publications_standards/publications/rights/index.html for more information.

This article has been accepted for publication in a future issue of this journal, but has not been fully edited. Content may change prior to final publication. Citation information: DOI 10.1109/JLT.2018.2879483, Journal of Lightwave Technology

the amplitude distortion is also well compensated as is shown in Fig. 8(d) and the amplitude ripple is restricted within 1.45 dB.

The pulse compression is done through digital signal processing (DSP). To make the comparison prominent, the Kaiser window is applied in each case. The pulse compression results are exhibited in Fig. 9. For the LFMW in the DSB-based link, the serious amplitude distortion caused by CD leads to the pulse fission as can be seen in Fig. 9(b). For the SSB case, the CD-induced phase distortion broadens the main lobe and raises the side lobes simultaneously. Compared with the uncorrupted input signal, the MLW is broadened by 0.45 ps, and the PSR is worsened by 3.23 dB as is shown in Fig. 9(c). In comparison, with the aid of the MPE, the MLW is barely broadened and the PSR only has a 0.19 dB deterioration, which verifies the effectiveness of our scheme.

V. Discussion

A. Amplitude ripple of the MPE-based link

According to (14), the amplitude of the LFMW in the MPE-based link is the function of three parameters, which are θ_1, θ_2 and τ. To demonstrate the amplitude ripple function of these three parameters, we perform the amplitude ripple tolerance test in simulation, in which we sweep one parameter and fix the other two, then the amplitude ripple is calculated and shown in Fig. 10. Here, we use the 80 km transmission case as an example, where the optimal parameters of the MPE are $\theta_1 = 0.71\pi$, $\theta_2 = -0.2\pi$ and $\tau = 4\text{ps}$.

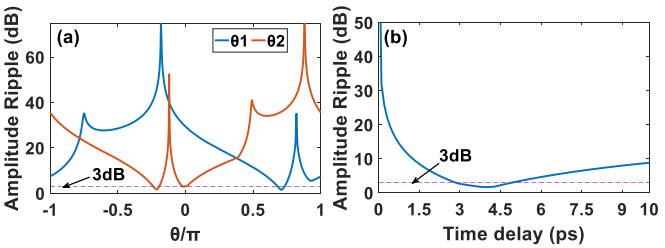

Fig. 10. Amplitude ripple performance as a function of (a) θ_1, θ_2 and (b) τ in the MPE-based link for the 80 km transmission case.

From the results presented in Fig. 10, we can see that the amplitude ripple is more sensitive to θ_1 and θ_2. By contrast, the time delay τ is a less sensitive parameter and has a larger operation range in order to alleviate the amplitude ripple less than 3dB.

B. Comparison of phase distortion

According to previous analysis, the amplitude distortion in the conventional DSB link can be well compensated by SSB and MPE techniques and the pulse fission can be avoided for the wideband LFMW. However, both SSB-based and MPE-based links will introduce phase distortion to wideband signals. Therefore, it is necessary to discuss and compare the phase distortion that the wideband LFMW will experience in three different links.

For traditional DSB-based links, the CD-induced relative phase difference between the sidebands and the optical carrier results in the amplitude distortion and the phase error is 0.

For the SSB-based link, according to Eq. (9), the CD-induced phase distortion introduces an additional phase and changes the chirp rate. In such a situation, the phase error can be expressed as:

$$\begin{aligned}\psi_{SSB}(\omega) &= -\frac{(\omega-\omega_s)^2}{k/(1-\beta_2 Lk/2)} - \frac{1}{2}\beta_2 L\omega_s^2 + \frac{(\omega-\omega_s)^2}{k} \\ &= \frac{1}{2}\beta_2 L(\omega-\omega_s)^2 - \frac{1}{2}\beta_2 L\omega_s^2\end{aligned} \tag{15}$$

For the MPE-based link, according to Eq. (13), the output LFMW field is:

$$I_{MPE}(\omega) = \left|I_{MPE}(\omega)\right| \exp[j\psi_{MPE}(\omega)] I_{in}(\omega) \tag{16}$$

where $\psi_{MPE}(\omega)$ is the phase error and it can be expressed as:

$$\begin{aligned}\psi_{MPE}(\omega,\tau) &= -\frac{\cos[\phi(\omega)-\theta_1]\sin(\omega\tau)}{\cos[\phi(\omega)-\theta_1]\cos(\omega\tau)+\cos[\phi(\omega)-\theta_2]} \\ &= -\frac{\sin(\omega\tau)}{\cos(\omega\tau)+\cos[\phi(\omega)-\theta_1]/\cos[\phi(\omega)-\theta_2]}\end{aligned} \tag{17}$$

According to our simulation results in section III, although the time delay τ is indispensable to mitigate the amplitude ripple, it is usually in the order of a few picoseconds (~10^{-12} s). As the maximum frequency of the wideband signal is tens of gigahertz (~10^9 GHz), $\sin(\omega\tau) \approx \omega\tau \ll 1$ is satisfied so that the phase distortion is less prominent.

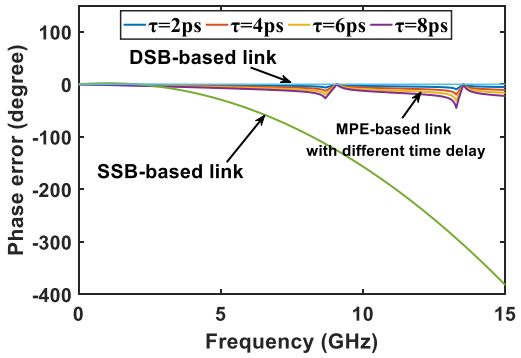

Fig. 11. Comparison of phase error in three links, as the function of frequency.

For comparison, we draw the phase error curves of the three links as the function of frequency for the 80 km fiber transmission case. Besides, as the MPE-induced phase error is a function of τ, the phase error curves for the MPE-based link with different values of τ are also plotted. As is shown in Fig. 11, the signal transmitted in the SSB link will experience more severe phase distortion, especially in the high-frequency part. For the MPE-based link, with the increase of τ, the phase error introduced by MPE becomes larger but still much smaller than that in SSB-based link, which shows the MPE's superiority over the SSB technique. For the wideband signals, which are sensitive to phase distortion such as the LFMW, the phase error caused by the SSB link will introduce serious performance deterioration to the signal, which can be verified in the next sub-section.

C. Comparison of Pulse compression performance

As the wideband LFMW is such a signal that is sensitive to both amplitude and phase distortion, which can be verified by

Copyright (c) 2015 IEEE. Personal use of this material is permitted. However, permission to use this material for any other purposes must be obtained from the IEEE by sending a request to pubs-permissions@ieee.org.

0733-8724 (c) 2018 IEEE. Personal use is permitted, but republication/redistribution requires IEEE permission. See http://www.ieee.org/publications_standards/publications/rights/index.html for more information.

This article has been accepted for publication in a future issue of this journal, but has not been fully edited. Content may change prior to final publication. Citation information: DOI 10.1109/JLT.2018.2879483, Journal of Lightwave Technology

the pulse compression performance, here we use the 1-15 GHz LFMW as an example and compare its performance degradation in DSB-based, SSB-based and MPE-based links to make an assessment of the anti-dispersion performance of the proposed MPE.

As is mentioned previously, the quality of the LFMW can be evaluated by MLW and PSR in pulse compression. Thus, the performance of the LFWM transmitted in three links is shown in Fig. 12, where the MLW and the PSR are plotted as functions of the SMF length.

For the conventional DSB-based link, when the LFMW is transmitted over a short distance (less than 30 km), the signal experiences slight distortion and the CD-induced amplitude distortion is equivalent to a window, which broadens the MLW and increases the PSR. With the increase of the fiber length, the signal undergoes more serious amplitude distortion and the MLW has a sharp increase. The compressed pulse finally splits into two pulses when the transmission distance reaches 30 km. Consequently, a ghost target will be introduced.

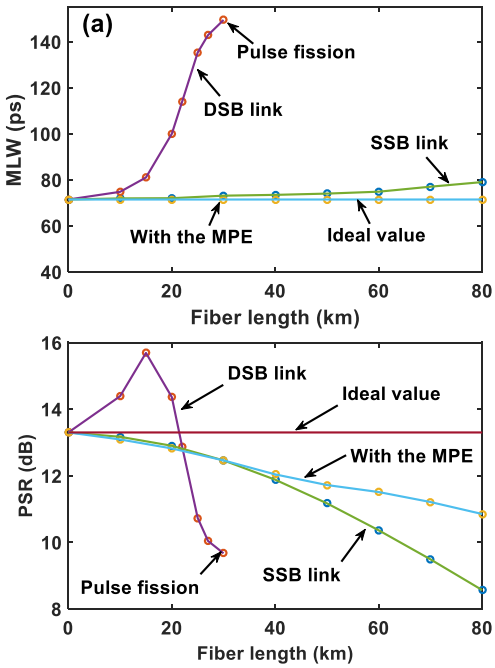

Fig. 12. (a) MLW and (b) PSR in the pulse compression of the three links, as functions of fiber length.

By contrast, since the SSB modulation can remove the CD-induced amplitude distortion, the pulse fission is avoided for the LFMW transmitted in the SSB-based RoF link. However, the fiber-induced CD distorts the phase of the LFMW and consequently broadens the main lobe of the compressed pulse. Compared with the DSB case, the broadening trend of the MLW is much milder, as is presented in Fig. 12(a). Meanwhile, as is shown in Fig. 12(b), the PSR is also deteriorated owing to CD, which causes difficulty in small targets detection.

As mentioned above, both CD-induced amplitude and phase distortions can be well compensated simultaneously with the help of the MPE. Therefore, as is shown in Fig. 12(a), the MLW is independent of fiber length and equals to the ideal value. Unfortunately, the slight phase error which is introduced by the relative time delay between the two taps leads to the deterioration of PSR, as is shown in Fig. 12(b). Even so, the compressed pulse of the output LFMW still has a better PSR in the MPE-based RoF link compared with the SSB case. Noting that, since there is no degradation in MLW, it is more appropriate (compared with the SSB case) to use the window processing so that a better PSR can be achieved.

In summary, thanks to the MPE, the wideband signal can be transmitted over the long-haul RoF link with negligible CD-induced distortions and can have a better performance compared with the signal transmitted in the DSB-based and SSB-based links.

VI. Conclusion

In conclusion, the CD-induced amplitude distortion in the conventional DSB-based RoF link and phase distortion in the SSB-based RoF link on wideband signal are theoretically studied through the analysis of the wideband LFMW. Subsequently, an MPE for overcoming the CD-induced distortions is proposed and its operating principle is demonstrated. In the proof-of-concept experiment, a 1-10 GHz LFMW is transmitted over the 66.3 km SMF in the MPE-based link with negligible distortions and the output signal has a better performance compared with the DSB and SSB cases. Moreover, the MPE has a relatively integrated structure, which is convenient to use and cost-effective. We believe this MPE will have its positions in distributed high-resolution radar systems, high-speed optical communications and broadband wireless access systems.

Appendix

TABLE I
Acronyms

Acronyms	Full name
CD	Chromatic dispersion
RF	Radio frequency
LFMW	Linear frequency modulated waveform
DSB	Double sideband
SSB	Single sideband
CPS-DSB	Carrier phase-shifted DSB
DGD	Differential group delay
MPE	Microwave photonics equalizer
MZM	Mach-Zehnder modulator
DPMZM	Dual-parallel MZM
DP-DPMZM	Dual-polarization DPMZM
SMF	Single-mode fiber
RoF	Radio-over-fiber
MLW	Main lobe width
PSR	Peak sidelobe ratio

Copyright (c) 2015 IEEE. Personal use of this material is permitted. However, permission to use this material for any other purposes must be obtained from the IEEE by sending a request to pubs-permissions@ieee.org.

0733-8724 (c) 2018 IEEE. Personal use is permitted, but republication/redistribution requires IEEE permission. See http://www.ieee.org/publications_standards/publications/rights/index.html for more information.

This article has been accepted for publication in a future issue of this journal, but has not been fully edited. Content may change prior to final publication. Citation information: DOI 10.1109/JLT.2018.2879483, Journal of Lightwave Technology

REFERENCES

[1] Yao, Jianping, "Microwave photonics," *J. Lightw. Technol.*, no. 3, pp. 314-335, Feb. 2009.

[2] H. Schmuck, "Comparison of optical millimeter-wave system concepts with regard to chromatic dispersion," *Electron. Lett.*, vol. 31, no. 21, pp. 1848–1849, Oct. 1995.

[3] U. Gliese, *et al*., "Chromatic dispersion in fiber-optic microwave and millimeter-wave links," *IEEE Trans. Microw. Theory Tech.*, vol. 44, no. 10, pp. 1716-1724, 1996.

[4] L. Grüner-Nielsen *et al*., "Dispersion-compensating fibers," *J. Lightw. Technol.*, vol. 23, no. 11, pp. 3566–3579, Jan. 2005.

[5] K. O. Hill *et al*., "Chirped in-fiber Bragg grating for compensation of optical-fiber dispersion," *Opt. Lett.*, vol. 19, pp. 1314–1316, 1994.

[6] C. K. Madsen and G. Lenz, "Optical all-pass filters for phase response design with applications for dispersion compensation," *IEEE Photon. Technol. Lette.*, vol. 10, p. 994, 1998.

[7] G. H. Smith *et al*., "Overcoming chromatic-dispersion effects in fiber-wireless systems incorporating external modulators," *IEEE Trans. Microw. Theory Tech.*, vol. 45, no. 8, pp. 1410–1415, Aug. 1997.

[8] S. R. Blais and J. P. Yao, "Optical single sideband modulation using an ultranarrow dual-transmission-band fiber Bragg grating," *IEEE Photon. Technol. Lett.*, vol. 18, no. 21, pp. 2230–2232, Nov. 2006.

[9] B. Hraimel *et al*., "Optical single-sideband modulation with tunable optical carrier to sideband ratio in radio over fiber systems," *J. Lightw. Technol.*, vol. 29, no. 5, pp. 775–781, Mar. 2011.

[10] Perez-Martinez *et al*., "Group delay effects on the performance of wideband CW-LFM radars." in *Proc. Inst. Elect. Eng.*, vol. 148, no. 2, pp. 95–100, Apr. 2001.

[11] S. Li, *et al*., "Compensation of dispersion-induced power fading for highly linear radio-over-fiber link using carrier phase-shifted double sideband modulation," *Opt. Lett.*, vol. 36, no. 4, pp. 546–548, Feb. 2011.

[12] H. Zhang *et al*., "Polarization-modulated analog photonic link with compensation of the dispersion-induced power fading," *Opt. Lett.*, vol. 37, no. 5, pp. 866–868, Mar. 2012

[13] Y. Gao *et al*., "Compensation of the dispersion-induced power fading in an analog photonic link based on PM-IM conversion in a Sagnac loop," *J. Lightw. Technol.*, vol. 33, no. 13, pp. 2899–2904, Jul. 2015.

[14] Y. Gao *et al*., "An analog photonic link with compensation of dispersion-induced power fading," *IEEE Photon. Technol. Lett.*, vol. 27, no. 12, pp. 1301–1304, Jun. 2015.

[15] V. J. Urick and F. Bucholtz, "Compensation of arbitrary chromatic dispersion in analog links using a modulation-diversity receiver," *IEEE Photon. Technol. Lett.*, vol. 17, no. 4, pp. 893–895, Apr. 2005.

[16] Z. Chen *et al*. "Dispersion compensation in analog photonic link utilizing a phase modulator," *J. Lightw. Technol.*, vol. 32, no. 23, pp. 4642–4647, Dec. 2014.

[17] Niu, Jian *et al*. "Broadband dispersion-induced power fading compensation in long-haul analog optical link based on 2-Ch phase modulator," *IEEE Photon. J.* , vol. 4, no. 2, pp. 476-482, Apr. 2012.

[18] V. J. Urick and F. Bucholtz, "Modulation diversity for chromatic dispersion compensation in analog photonic links," *Photon. Technol. Branch Opt. Sci. Div.*, 2006.

[19] Y. Le Guennec *et al*., "Technologies for UWB-over-fiber," in *Proc. Annu. Meeting IEEE Lasers Electro Opt. Soc.*, Oct. 2006, pp. 518–519.

[20] M. Ran *et al*., "Ultra-wideband radio-over-optical fiber concepts, technologies and applications," *IEEE Photon. J.*, vol. 2, no. 1, pp. 36–48, Feb. 2010.

[21] S. Pan and Y. Yao, "UWB-over fiber communications: Modulation and transmission," *J. Lightw. Technol.*, vol. 28, no. 16, pp. 2445–2455, Aug. 2010.

[22] W. Shieh *et al*., "Performance of a 12-kilometer photonic link for X-band antenna remoting in NASA's deep space network," *Telecommun. Mission Oper. Prog. Rep.*, vol. 138, pp. 1–8, 1999.

[23] J. E. Román *et al*., "Fiber-optic remoting of an ultrahigh dynamic range radar," *IEEE Trans. Microw. Theory Tech.*, vol. 46, no. 12, pp. 2317–2323, Dec. 1998.

[24] M. I. Skolnik Ed., *Radar Handbook*, 2nd ed. New York, NY, USA: McGraw-Hill, 1991.

[25] B. Levitas and J. Matuzas, "UWB radar high resolution ISAR imaging," in *Second International Workshop Ultrawideband and Ultrashort Impulse Signals*, Sep. 19–22, 2004, pp. 228–230.

[26] S. Peng *et al*., "High-resolution W-band ISAR imaging system utilizing a logic-operation-based photonic digital-to-analog converter," *Opt. Exp.*, vol. 26, pp. 1978-1987, 2018.

Copyright (c) 2015 IEEE. Personal use of this material is permitted. However, permission to use this material for any other purposes must be obtained from the IEEE by sending a request to pubs-permissions@ieee.org.

0733-8724 (c) 2018 IEEE. Personal use is permitted, but republication/redistribution requires IEEE permission. See http://www.ieee.org/publications_standards/publications/rights/index.html for more information.